

A physically modelled selection function for compact binary mergers in the LIGO-Virgo O3 run and beyond

Ana Lorenzo-Medina¹, Thomas Dent¹

¹ Instituto Galego de Física de Altas Enerxías, Universidade de Santiago de Compostela, 15782 Santiago de Compostela, Galicia, Spain

E-mail: analorenzo.medina@usc.es, thomas.dent@usc.es

Abstract. Despite the observation of nearly 100 compact binary coalescence (CBC) events up to the end of the Advanced gravitational-wave (GW) detectors' third observing run (O3), there remain fundamental open questions regarding their astrophysical formation mechanisms and environments. Population analysis should yield insights into these questions, but requires careful control of uncertainties and biases. GW observations have a strong selection bias: this is due first to the dependence of the signal amplitude on the source's (intrinsic and extrinsic) parameters, and second to the complicated nature of detector noise and of current detection methods. In this work, we introduce a new physically-motivated model of the sensitivity of GW searches for CBC events, aimed at enhancing the accuracy and efficiency of population reconstructions. In contrast to current methods which rely on re-weighting simulated signals (injections) via importance sampling, we model the probability of detection of binary black hole (BBH) mergers as a smooth, analytic function of source masses, orbit-aligned spins, and distance, fitted to accurately match injection results. The estimate can thus be used for population models whose signal distribution over parameter space differs significantly from the injection distribution. Our method has already been used in population studies such as reconstructing the BBH merger rate dependence on redshift.

1. Introduction

Gravitational wave (GW) astronomy has made a number of breakthroughs in recent years, with the first detection of merging black holes by the interferometric gravitational-wave detector network on 14 September 2015 [1]. Coalescences of compact binaries (CBC), such as black hole or neutron star binaries, are a particularly interesting source for broadband detectors, since the signal from an inspiral is quite strong compared to other types of GWs, and the binary system properties can be measured with high precision for some parameters of astrophysical interest, due to the large number of signal cycles observable in the sensitive frequency band [2]. With the current catalog of close to 100 observed binaries [3] many unanswered questions about such sources remain, such as the origin of GW-emitting black hole binary (BBH) systems, it being debatable whether they have properties different from [4] or similar to [5] black holes detected via X-ray emission.

Many formation channels and mechanisms have been proposed for the BBH observed via GW emission (see [6] for an overview). Among the most intensively studied are isolated binary evolution (e.g. [7, 8], and dynamical binary formation in globular or other stellar clusters (e.g. [9, 10]) or around galactic centres (e.g. [11]). Each of these channels may have distinctive signatures in the distribution of merging binaries over masses, spins and redshift, though subject to many theoretical and modelling uncertainties (e.g. [12]; see [13, 14, 15] for more detailed discussion). Currently, no single formation channel appears capable of explaining the entire population [16], implying that a more complex mixture of channels will eventually be crucial to properly describe observations. The current detector network is only sensitive over a limited range of redshift: thus, although some studies find hints of population evolution over cosmic history, such findings are so far strongly dependent on the choice of methods [17, 18, 19, 20, 21]. Since various formation channels are expected to have different dependencies on redshift [22, 23, 24], tracking such evolution will become increasingly important to untangle them as detector sensitivity increases (e.g. [25]).

The set of binary mergers that we observe comes with a significant bias as compared to the actual astrophysical BBH population, because of selection effects, which are crucial to take into account in population studies (see e.g. [26] for an early review). The most direct selection effect, and the one currently limiting our ability to probe cosmic evolution, is that nearby (low redshift) sources are more likely to be detected than far (high redshift) ones. Nearly as important is the dependence of signal amplitude on binary masses: for the inspiral phase of the signal, this varies as (a power of) the chirp mass $\mathcal{M} = (m_1 m_2)^{3/5} / (m_1 + m_2)^{1/5}$, while for the later merger-ringdown phase the binary total mass has the most influence. The spins of binary components also affect the GW signal detectability [27, 28], primarily via a longer or shorter signal duration with the merger at higher (lower) frequency for spins aligned (anti-aligned) with the orbit. Spins in the plane of the orbit, which give rise to precession effects, also affect detection, primarily since the existing searches use templates with only orbit-aligned component spins, which therefore cannot fully match signals with precession (e.g. [29]); similar considerations apply to non-dominant multipole (“higher mode”) emission which is not included in current template banks [30, 31]. Signals from binaries with non-negligible residual orbital eccentricity will also be less efficiently recovered [32, 33]; studies of eccentricity in combination with other effects will eventually be required, with accurate waveform modelling as a technical limiting factor (see e.g. discussions in [34]).

The interplay of search sensitivity with these astrophysical properties of binaries makes

it crucial to have an accurate quantitative estimate of selection effects when carrying out population analysis. This is provided by an estimate of the probability of detection P_{det} , or selection function, of binary mergers: an accurate estimate enables measurement of the rates of binary merger events, and reconstruction of their population distribution as a function of component masses, spins and redshift [13, 14].

Events are considered to be detected on the basis of their statistical significance assigned by search pipelines, i.e. matched-filtering algorithms looking for signals in the data [35, 36, 37, 38, 39]. Each candidate event has a ranking statistic value calculated as a predefined function of the event parameters. The significance may be quantified by the false alarm rate (FAR), which is the expected rate of candidates in the pipeline resulting from detector noise which are ranked equal to or higher than the candidate under consideration. A set of candidates of well defined purity, in terms of the expected number of noise events, may be obtained by imposing a pre-defined maximum threshold on FAR. BBH candidates have typically been considered for population analysis if their FAR is below a threshold 1/yr; in the case of several pipelines, one may apply the threshold to the most significant result between pipelines for a given candidate [13, 14].[‡]

The detection fraction of a population described by a model PDF $\pi(\theta|\Lambda)$ with (hyper)parameters Λ is a crucial element in population inference (e.g. [42, 43]): it is defined by

$$\xi(\Lambda) = \int P_{\text{det}}(\theta) \pi(\theta|\Lambda) d(\theta), \quad (1)$$

where $P_{\text{det}}(\theta)$ stands for the probability that an event with parameters θ would be detected (found) by a particular search or a combination of searches. For binary population analyses, P_{det} is estimated indirectly by simulating CBC signals from a reference BBH population, adding them to real detector data and analysing the “injected” data with search pipelines to record which ones are detected [14]. For the detection fraction to be well defined, we must restrict the time of arrival (considered as an event parameter) to periods where any detectors were observing, and effectively calculate average detectability over such periods.

Since the previous integral cannot be evaluated analytically, importance sampling may be used instead to estimate it using a weighted Monte Carlo integral (see e.g. [44]) over found injections, i.e. those satisfying the chosen search significance threshold:

$$\hat{\xi}(\Lambda) = \frac{1}{N_{\text{inj}}} \sum_{j=1}^{N_{\text{det}}} \frac{\pi(\theta_j|\Lambda)}{p_{\text{draw}}(\theta_j)} \equiv \frac{1}{N_{\text{inj}}} \sum_{j=1}^{N_{\text{det}}} w_j, \quad (2)$$

in which N_{inj} is the total number of injections, $j = 1, \dots, N_{\text{det}}$ labels the found (detected) injections, and p_{draw} is a fiducial distribution from which the samples are drawn [45, 43].

Importance sampling is a convenient approach since it only requires one pre-determined injection analysis campaign to be performed by searches, which is then used to estimate selection effects for any population models considered. However, this procedure comes with uncertainty in the estimation of the selection integral: the precision of the estimation depends on how well the proposal model π matches the form of p_{draw} . There must be enough

[‡] Other methods of quantifying event significance by pooling multiple pipeline results may be considered [40, 41].

samples drawn and detected by search pipelines so that this uncertainty does not alter the shape of the population model posterior [43, 46, 47]. The precision may be quantified via the effective number of independent draws (sample size), N_{eff} , that contribute to estimate ξ for a given model. This effective sample size is defined as the square of the estimated fraction $\hat{\xi}$ divided by its variance due to Monte Carlo uncertainty [47]; in terms of the weights $w_j = \pi(\theta_j)/p_{\text{draw}}(\theta_j)$, N_{eff} varies as

$$\frac{\hat{\xi}^2}{\text{Var}(\hat{\xi})} \equiv N_{\text{eff}} \simeq \frac{(\sum_j w_j)^2}{\sum_j w_j^2}. \quad (3)$$

Then depending on the model $\pi(\theta|\Lambda)$, for a fixed injection set N_{eff} may or may not be high enough to obtain an accurate population inference; as a general guide $N_{\text{eff}} > 4N_{\text{obs}}$ has been required (where N_{obs} is the number of events in the population catalog) [43, 46]. Then, if we discount the possibility of requiring more injections to be analyzed ad-hoc, in general at high computational cost, a large class of models cannot be studied using a generic (broadly/uniformly distributed) injection set [47]. For example, population models where $\pi(\theta|\Lambda)$ is strongly peaked around a specific point, if the density of injections $p_{\text{draw}}(\theta)$ is featureless (e.g. [48]); or in general, where some w_i are $\gg 1$ (see also [49]).

As an alternative, using an analytical function – or in general, a continuous function – that accurately describes the probability of detection of BBH signals will make it possible to estimate P_{det} without such restrictions on the model and original injection sampling distributions. As an initial effort towards such a description, the dependence on masses and spins of the selection function can be modelled via “semi-analytic” methods with various possible corrections. The interferometer network sensitivity is approximated by evaluating the expected (optimal) signal-to-noise ratios (SNRs) of signals for fixed, ideal detector power spectral densities (PSDs). The probability of detection is then obtained by assuming that the network is sensitive to CBCs with SNR above a fiducial threshold value [26, 50], which may be tuned to approximate the number of actual signals, or injections detected by search pipelines [51, 52].

However, a simple optimal SNR threshold is not necessarily an accurate approximation for P_{det} , due to many factors which violate the assumptions behind the “semi-analytic” calculation. Beyond the effect of the noise realization on matched filter SNR (e.g. [52]), for instance, the number of detectors observing and their sensitivity varies over time [53, 54, 55, 56]; detector noise is also not completely described by a single set of PSDs, being not perfectly Gaussian and stationary. In reality there are excess noise transients (“glitches”, see e.g. [57, 58]) that may be partly suppressed by search pipelines employing additional quantities beyond the SNR, and other non-ideal noise behaviour [59, 60]. In general the search ranking statistic may have additional dependences beyond the SNR, for example explicit dependence on masses and/or spins [61, 62]§, and/or on detector outputs other than strain which are correlated with transient noise [64, 65, 66].

Hence, corrections to the semi-analytic approach will in general be necessary. A simple grid-based approach to obtain such corrections by fitting the mass- and (aligned) spin-dependent sensitive volume, i.e. the integral of P_{det} over space properly weighted by comoving volume-time, to search injection results was developed in [67] and applied

§ Such dependence amounts to modelling a signal population for which the search is optimized [63]: like other aspects of the event ranking, this must be determined in advance of performing the search.

in [13, 14]. Machine learning techniques using density estimation on found injections to get a continuous and generative model for P_{det} were demonstrated in [68]; however, neither method was applied to obtain the distance or redshift dependence of P_{det} , which is crucial for cosmological investigations such as [21]. One obstacle to directly estimating $P_{\text{det}}(d_L)$ is the sparsity of injections at small distances, if distributed with (comoving) volume.

The strategy we pursue here to overcome this limitation is to fit a continuous and physically motivated P_{det} function over distance, masses and, ultimately, spins. While the basic functional form is derived from the known theoretical dependence of SNR on distance and chirp mass, we introduce corrections to account for non-ideal detector behaviour, and for higher order effects of masses and spins on an event’s detectability in actual search pipelines. The fit is adjusted to maximize the likelihood of found injections in the O3 sensitivity data release corresponding to GWTC-3 [69, 3].

The remainder of the paper is structured as follows: in Section 2 we lay out the methods used in this work, as well as the functions derived to fit P_{det} accurately over masses and distance. In Sec. 3 we present the results obtained from the fit to the O3 injection set, and validate the first by comparison of CDFs and Kolmogorov-Smirnov (KS) tests. In Sec. 4 we add a dependence to P_{det} on the effective spin, and demonstrate a resulting improvement in the fit accuracy. In Sec. 5 we quantify the statistical uncertainties in our fitted function for P_{det} via bootstrap resampling. Finally, in Sec. 6 we summarize the work and discuss possible implications and further developments.

2. Methods

The aim of this project is to obtain accurate estimates of the selection function, or probability of detection, for gravitational-wave sources considering the only type of system so far detected, compact binaries of neutron stars or black holes. The selection function depends strongly on the properties of the binary components as well as the source’s distance from Earth, and thus on the redshift.

LIGO-Virgo-KAGRA (LVK) O3 BBH search sensitivity estimates [69] were used for the analysis. This data release contains sets of simulated signals (injections) from binary black holes that can be used to estimate the search sensitivity corresponding to the GWTC-3 catalog [70].

Regarding the analysis presented in this work we are considering the binary source component masses and redshift, hence the parameters determining the detectability of signals will be the redshifted masses m_{1z} , m_{2z} (masses in the detector’s frame) and the luminosity distance $d_L(z)$. Selection effects are thus described via a function $P_{\text{det}}(m_{1z}, m_{2z}, d_L)$ giving the probability of detection for a merger occurring during an observing period. The probability is understood to be marginalized over extrinsic (location and orientation) parameters, over time of arrival and over detector noise realizations, and also, in sections 2 and 3, over binary component spins.

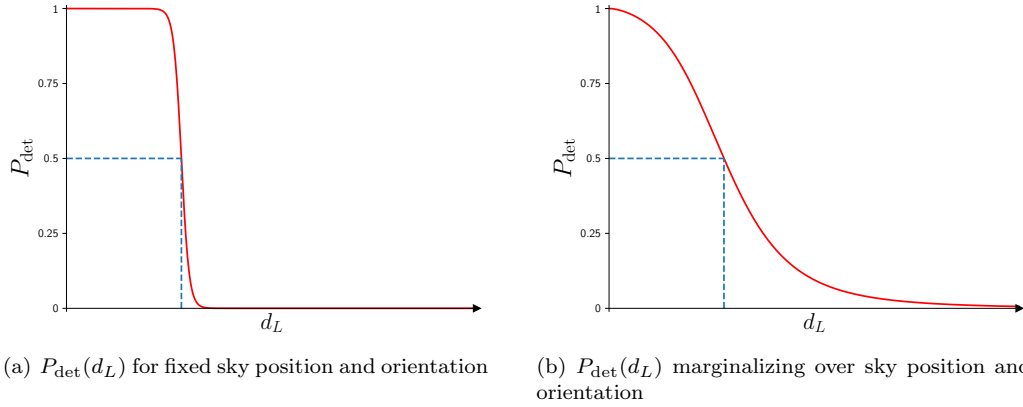


Figure 1. Schematic dependence of search sensitivity on luminosity distance for fixed binary intrinsic parameters. The blue dashed lines indicate d_{mid} , the distance at which detection probability falls to 0.5.

2.1. Sigmoid distance dependence model

Considering a source of fixed intrinsic parameters (binary component masses and spins), the dependence on distance of search sensitivity is mainly determined by the sky position and orientation of the source relative to a detector network (assumed to have stationary sensitivity), described by various angular parameters. If the angular parameters were also fixed, then the amplitude and expected SNR are simply inversely proportional to distance: then, assuming the source is detected if SNR is above a given threshold, $P_{\text{det}}(d_L)$ would be almost 1 for some range of distances up to a given point, and then close to 0 for larger distances, as represented in Fig. 1a. The detection probability has the shape of a sigmoid instead of a step function because of noise in the detector: in an actual search, detection will be determined by the matched filter SNR, a function of the data which contains a stochastic term resulting from the detector noise realization in addition to the expected SNR.

Since the sources' positions and orientations are *a priori* unknown, and isotropically distributed throughout the sky, we need to consider all the possible values of the angular parameters and average over them. As a result of this marginalization, the functional form of the search sensitivity takes a form more similar to Fig. 1b. These effects on search sensitivity were quantified by Finn & Chernoff (FC) [71], predicting the form of the probability of detection function over distance by considering geometrical factors in the expected SNR for the case of only one detector with fixed sensitivity.

Although the true functional dependence of $P_{\text{det}}(d_L)$ in a realistic case will have many corrections relative to this idealized calculation, our fundamental model assumption is that such corrections are small. Thus, as a starting point we use a parameterized sigmoid function that is able to fit the FC data ([71] Table I) faithfully, while also allowing for minor deviations. The shape of the sigmoid is controlled by four parameters ε_{max} , α , δ and γ , out of which $\alpha = 2.05$ is fixed to the value obtained in a direct fit to FC data and the other 3 will be free model parameters. The probability of detection, for a binary with given

intrinsic parameters, thus reads as

$$P_{\text{det}} = \frac{\varepsilon_{\text{max}}}{1 + \hat{d}_L^\alpha \exp \left[\gamma(\hat{d}_L - 1) + \delta(\hat{d}_L^2 - 1) \right]}, \quad (4)$$

where $\hat{d}_L \equiv d_L/d_{\text{mid}}$ is the luminosity distance, scaled by the “midpoint distance” d_{mid} at which the sigmoid falls to 50% of its maximum value, and ε_{max} gives the detection probability in the limit $d_L \rightarrow 0$. Specifically, within a given observing run, the adjustable parameters are intended to model the effects (averaged over the run) of both stationary Gaussian detector noise, and non-stationary behaviour affecting detector sensitivities, including the observation duty cycles of different detectors in the network.

Furthermore, we allow the search sensitivity in the limit of very loud signals ε_{max} to be less than 1, which may happen due to effects of precession, higher modes, etc., causing the GW signal to differ significantly from the templates used in searches (e.g. [72, 29, 30]); for published LVK results, such templates include only the dominant multipole emission from non-precessing binaries, as advocated in [27].

Having modelled the dependence on amplitude and distance for fixed intrinsic binary parameters, we then add a dependence on these intrinsic parameters by writing $d_{\text{mid}}(m_{1z}, m_{2z})$ and $\varepsilon_{\text{max}}(m_{1z}, m_{2z})$ as a function of the redshifted masses (we will also allow for component spin dependence in Sec. 4). In the low mass limit, d_{mid} is expected to take the form $d_{\text{mid}} \sim D_0 f_d \mathcal{M}_z^{5/6}$, where D_0 is a constant corresponding to average detector sensitivity over a given observing run; i.e. sensitive distance should scale with $\mathcal{M}_z^{5/6}$ for the simplest inspiral model, where the redshifted chirp mass is given by $\mathcal{M}_z = \eta^{3/5} M_z$ in terms of the redshifted binary total mass $M_z = m_{1z} + m_{2z}$ and the symmetric mass ratio $\eta = m_1 m_2 / M^2 \equiv m_{1z} m_{2z} / M_z^2$. The remaining dependence on masses, corresponding to corrections to this lowest order inspiral SNR power law behaviour, is then to be fitted by a function $f_d(M_z, \eta)$. Taking into account that ε_{max} should not be higher than 1 and always positive, we take a functional form $\varepsilon_{\text{max}} \sim 1 - \exp(f_\varepsilon)$, with f_ε a function of intrinsic parameters.

At this point, the functions providing mass dependence to d_{mid} and ε_{max} could be any arbitrary combination of M_z and η . In order to gain more insight into the needed corrections, we perform mass binned fits to the detected injections released with the GWTC-3 catalog.

2.2. Mass binned fits

In order to gain insight into the functional forms of f_d and f_ε that will be able to fit injection results over the BBH mass space, we first fit our analytical model of P_{det} as a function of distance for fixed masses, or rather in mass bins, by numerically maximizing the likelihood of the injection campaign search results.^{||} In this binned fit procedure, rather than being continuous functions, d_{mid} and ε_{max} are treated as scalar parameters, fitted separately for each mass bin; we choose bins equally spaced in the logarithms of m_1 and m_2 , as they then contain comparable counts of found injections with $\text{FAR} \leq 1/\text{yr}$ [14], at least for mass

^{||} Code to evaluate our P_{det} model and fit its parameters to injection results, and the resulting maximum likelihood parameter values, are publicly available at https://github.com/AnaLorenzoMedina/cbc_pdet.

ratios close to unity. For a given mass bin labeled as \cdot^M we use a inhomogeneous Poisson likelihood for the found injections:

$$\ln \mathcal{L}^M = -\mu^M + \sum_i \ln \lambda^M(d_L^i), \quad (5)$$

where λ^M stands for the expected density of found injections at a given distance,

$$\lambda^M(d_L) = P_{\text{det}}(d_L) p(d_L) N_{\text{tot}}^M, \quad (6)$$

where $P_{\text{det}}(d_L)$ is evaluated using given values of d_{mid} and ε_{max} ; we write $N_{\text{tot}}^M = N_{\text{total}} \iint p(m_1, m_2) dm_1 dm_2$ for the expected total number of injections in the bin, where the distributions $p(\theta)$ are the sampling probability density functions (pdf) for $\vec{\theta} = \{m_1, m_2, d_L\}$ (described in Appendix A for O3 injections), N_{total} is the total number of injections originally generated, and μ stands for the expected total number of found injections in the bin:

$$\mu^M \equiv N_{\text{exp}} = \int_0^\infty \lambda^M(d_L) dd_L. \quad (7)$$

Although d_{mid} and ε_{max} vary between bins, we use the same shape parameter values δ and γ over the whole mass range, since we assume P_{det} should have the same shape regardless of the mass. We then perform a fit in two alternating stages. In the ‘sigmoid fitting’ stage, d_{mid} and ε_{max} are held fixed for all bins and the sigmoid shape is fitted by maximizing the total log likelihood $\sum_M \ln \mathcal{L}^M$ over δ and γ . In the ‘mass fitting’ stage, δ and γ are instead fixed and the values of d_{mid} and ε_{max} are fitted separately for each bin by maximizing $\ln \mathcal{L}^M$. The two stages are alternated until the total likelihood has converged to a global maximum (see e.g. [73] for a general discussion of “alternating optimization”). For optimization at each stage the Nelder-Mead simplex algorithm was used, a typical direct search method for multidimensional unconstrained minimization (e.g. [74]).

Figure 2 shows the resulting optimized values of d_{mid} , having scaled out a factor of $\mathcal{M}_z^{5/6}$. While all the values are comparable in magnitude, we see strong linear and quadratic dependencies on M_z at higher η , decreasing as the symmetric mass ratio gets smaller. Taking into account this behaviour, we first proposed the following expression to describe the global mass dependence:[¶]

$$d_{\text{mid}}^*(m_{1z}, m_{2z}) = D_0 \mathcal{M}_z^{5/6} [1 + a_{10} M_z + a_{20} M_z^2 + (a_{01} + a_{11} M_z + a_{21} M_z^2)(1 - 4\eta)], \quad (8)$$

in which we are separating out the dependence away from equal masses (i.e. for $\eta < 1/4$) where there may be higher uncertainty, treating this as a correction for unequal mass binaries. This first fit was already used in a population analysis to investigate the evolution of the BBH population over redshift [21]. However this function has the disadvantage that it may become negative, which would be physically disallowed; therefore for our main results we use a slightly modified form with corrections via an exponential:

$$d_{\text{mid}}(m_{1z}, m_{2z}) = D_0 \mathcal{M}_z^{5/6} \exp(f_d), \quad (9)$$

$$f_d = a_{10} M_z + a_{20} M_z^2 + (a_{01} + a_{11} M_z + a_{21} M_z^2)(1 - 4\eta). \quad (10)$$

[¶] The a coefficient subscripts, in order, represent powers of M_z and $(1 - 4\eta)$.

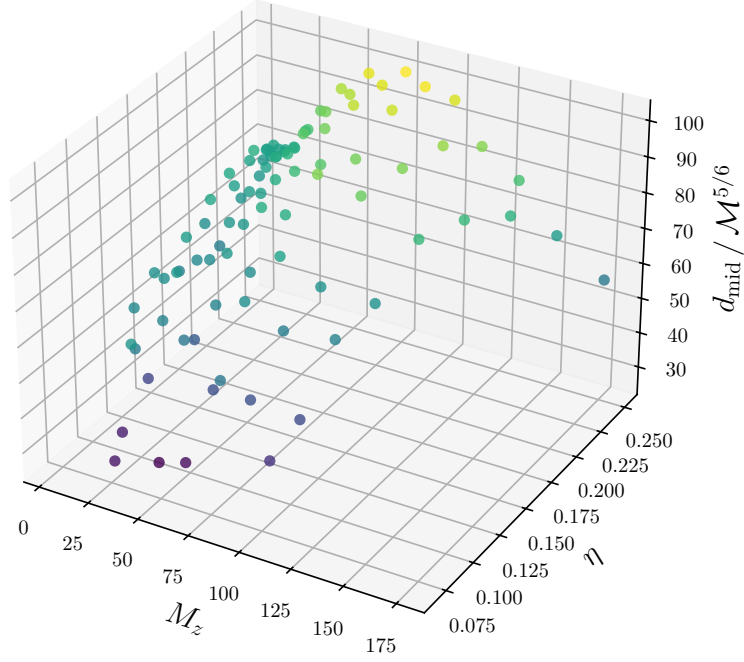


Figure 2. Optimized sensitive distance d_{mid} estimates from the mass binned fits. Points are colored according to the z-axis values $d_{\text{mid}}/M_z^{5/6}$ for clarity.

We next consider the functional dependence of ε_{max} (the detection probability in the limit of zero distance) by inspecting the optimized values of ε_{max} for binned fits in Fig. 3. Here, we allow (in principle unphysical) ε_{max} values greater than 1 which may be caused by small number statistics; although the total number of found injections in a bin may be large, due to their distribution over distance, the detection probability at small distance is typically badly constrained. The trend of variation is most apparent over linear total mass, therefore given the restrictions stated previously we chose the following function:

$$\varepsilon_{\text{max}}(m_{1z}, m_{2z}) = 1 - \exp(b_0 + b_1 M_z + b_2 M_z^2). \quad (11)$$

2.3. Global fits: mass dependence

Given the functional forms of f_d and f_ε described in the previous section, we have everything we need to make a global fit, that is, obtain a smooth function of P_{det} in terms of both distance and masses. To optimize the parameters of the global function, the previous expressions for the likelihood need to be generalised:

$$\ln \mathcal{L} = -\mu + \sum_i \ln \lambda(d_L^i, m_1^i, m_2^i), \quad (12)$$

$$\lambda(d_L, m_1, m_2) = P_{\text{det}}(d_L, m_1, m_2) p(d_L) p(m_1, m_2) N_{\text{tot}}, \quad (13)$$

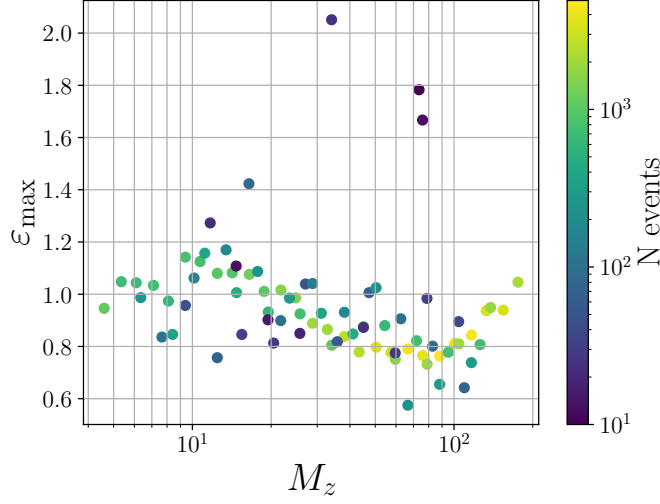


Figure 3. Maximum search efficiency ε_{\max} fitted values for each mass bin: the color bar shows the number of detected events (injections) in each bin.

$$\mu \equiv N_{\text{exp}} = \iiint \lambda(d_L, m_1, m_2) dm_1 dm_2 dd_L. \quad (14)$$

The triple integral in (14) could in principle be computed numerically, but at high computational cost. Instead, we obtain an accurate approximation from $N_{\text{exp}} \simeq \sum_i P_{\text{det}}(d_{Li}, m_{1i}, m_{2i})$, evaluating over all injections (both found and missed) as these are already correctly distributed as $p(d_L)p(m_1, m_2)$.

The sigmoid parameters γ and δ , as well as the new parameters from d_{mid} and ε_{\max} , were fitted to the GWTC-3 injections by maximizing the likelihood (12). Similarly to the binned fit, we perform optimization in two alternating steps. Firstly, the likelihood is maximized optimizing over the d_{mid} parameters, $\{D_0, a_{10}, a_{20}, a_{01}, a_{11}, a_{21}\}$, and the rest of them are fixed. In step two the optimization takes place over the parameters controlling the shape of the sigmoid curve, namely $\{\gamma, \delta, b_0, b_1, b_2\}$, using the optimized d_{mid} values gotten in step 1. Then the two steps are repeated until the difference in the log likelihood is less than 0.01, in order to ensure a stable maximum value.

3. Results and discussion

Figure 4(a) shows the values of d_{mid} obtained from the fit in terms of the redshifted masses, computed for every injection in the GWTC-3 catalog. The dependence on masses presents a local maximum around 3800 Mpc for $m_{1z}, m_{2z} \gtrsim 150 M_\odot$, which corresponds to redshifted chirp mass $\sim 150 M_\odot$, consistent with aLIGO expected sensitivity to compact binary coalescences [75]. For chirp masses below $\sim 150 M_\odot$ the sensitive distance increases with mass, mainly driven by a higher signal amplitude. However, the merger also shifts towards lower frequencies, eventually leaving the detectors' frequency band, thus the sensitive distance decreases for chirp masses $\gtrsim 150 M_\odot$. Moreover, higher mass signals

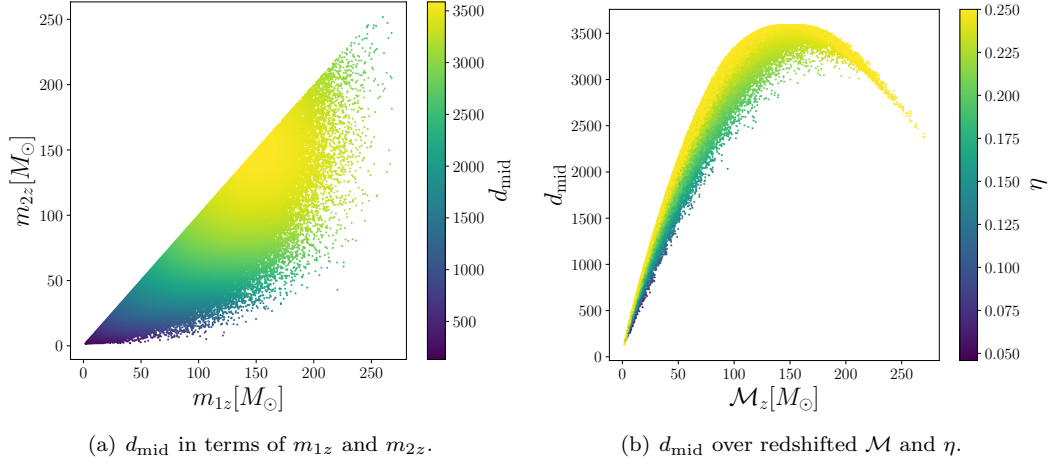


Figure 4. Sensitive distance d_{mid} values for the O3 BBH injections obtained from the global fit of P_{det} , plotted over redshifted masses m_{1z}, m_{2z} (a) and over redshifted chirp mass \mathcal{M}_z and symmetric mass ratio η (b).

have fewer cycles visible in band, thus being more readily mimicked by glitches: an effectively higher background for high-mass templates is therefore expected to contribute to decreasing sensitivity towards high masses. Figure. 4(b) shows behaviour consistent with these expectations, and also indicates a trend for higher (lower) sensitivity to equal (unequal)-mass binaries at a given chirp mass.

Maximum detection probability is plotted in Fig. 5(a) in terms of redshifted total mass, presenting an interesting behaviour for higher masses. The interpretation of the local minimum around $M_z \sim 400 M_\odot$ is not yet clear, since various different effects (precessing spins, non-dominant signal modes, higher glitch backgrounds) could lead to high-mass signals not being detected, even at very low distances: we further discuss spin effects in Sec. 4. However the number of injections performed at high masses is much smaller, let alone the number detected, making it difficult to obtain precise results in the large mass limit; statistical uncertainties will be discussed in detail in Sec. 5.

Lastly, Fig. 5(b) shows the probability of detection of every O3 BBH injection using the optimized parameters obtained from the global fit. Here, we plot distance rescaled to d_{mid} (i.e. removing most of the mass dependence), thus P_{det} follows a expected sigmoid shape going up to almost 1 for small d_L/d_{mid} values and becoming almost zero for very large distances.

3.1. Diagnostics: cumulative distributions

In order to check our choices of functional forms for both d_{mid} and ε_{max} , and also to validate the resulting fit, we compared the cumulative counts and (normalized) distributions (cdfs) of actual found injections in the GWTC-3 dataset over various parameters of interest with the cumulative counts or cdfs that are expected from the inferred selection function. The

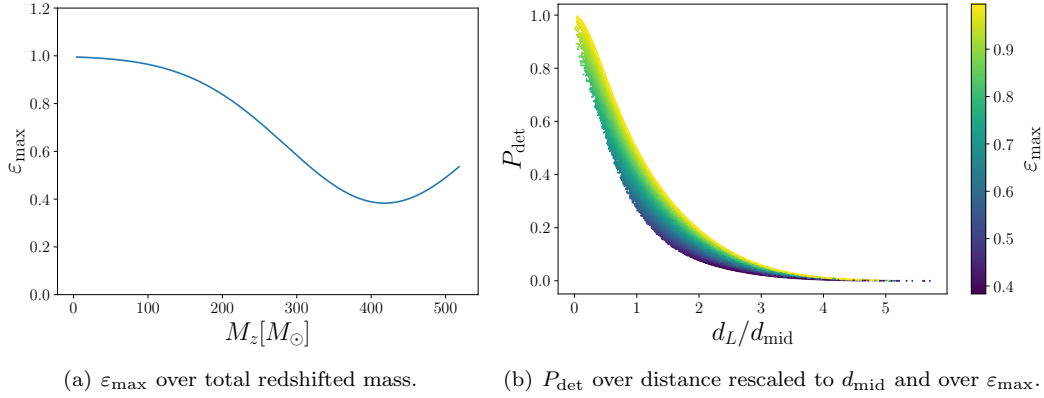


Figure 5. Mass dependence of the maximum detection probability ε_{\max} (a) and probability of detection over distance rescaled to d_{mid} , colored by ε_{\max} (b) for O3 BBH injections. The spread of points in (b) indicating a departure from a single universal function is caused by the mass dependence of ε_{\max} .

expected cdf of found injections is given by

$$\text{cdf}(\theta^*) = \frac{\int_{-\infty}^{\theta^*} P_{\text{det}}(\theta) p(\theta) d\theta}{\int_{-\infty}^{\infty} P_{\text{det}}(\theta) p(\theta) d\theta} \simeq \frac{\sum_{\theta_i \leq \theta^*} P_{\text{det}}(\theta_i)}{\sum_{\theta_i} P_{\text{det}}(\theta_i)}, \quad (15)$$

i.e. the probability of the parameter θ for a found injection taking on a value less than or equal to θ^* . We carried out comparisons for different variables θ : luminosity distance, symmetric mass ratio, total mass and chirp mass in both the source and the detector frame; for the sake of space, we only illustrate two here. Figure 6 compares the cumulative counts $\sum P_{\text{det}}(\theta_i)$ of found injections over luminosity distance and redshifted chirp mass, validating our P_{det} fit since the predicted found injections match almost perfectly the actual detected ones.

Lastly, Kolmogorov-Smirnov (K-S) tests were performed for each of the cdfs to quantify the accuracy of the fit. Over d_L , we obtained a K-S statistic of 0.0026 and a p -value of 0.65; similar results for \mathcal{M}_z , K-S statistic = 0.0044 and p -value = 0.098. Overall, all the K-S statistics values obtained were 0.004 or less, i.e. a maximum deviation $\leq 0.4\%$ of the actual from the predicted distribution, and p -values of 0.09 or larger, i.e. no significant discrepancies. Together, the present findings confirm that our model is able to accurately predict the number of found injections, and thus support the choice of the selection function. We are, though, unable to constrain or verify the behaviour of P_{det} outside the physical range of masses and distances covered by the injection set: in extreme cases (for instance binaries with mass ratio q as small as $\mathcal{O}(0.01)$) our model may yield an unphysical estimate. However its behaviour may readily be checked within the domain where, for instance, LVK give BBH merger rates estimates [14].

Even though these results show that the fit over the mass and distance degrees of freedom is good, we have ignored any dependence on spins. In fact, comparing cdfs and

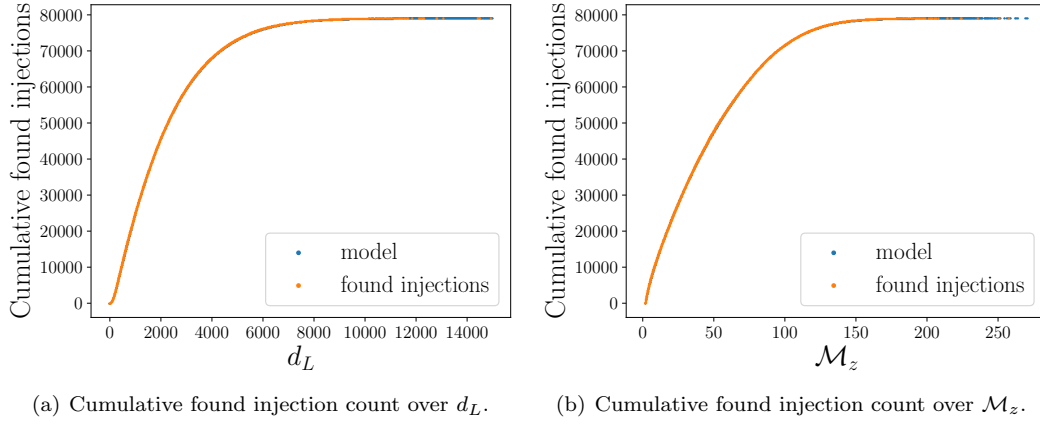


Figure 6. Cumulative found injections from the GWTC-3 data (orange) and the predicted cdf ('model') from Eq. (15) (blue), evaluating the model count at the parameter value of each injection.

performing K-S tests over spin variables shows significant discrepancies: this motivates including at least the leading dependence of search sensitivity on component spins, which we describe in the following section.

4. Inclusion of leading spin effects

Up to this point we are not taking into account spin effects, which would only be reasonable if we assume all black hole spins are small. Further work is needed in order to fit aligned spin dependence to the selection function, as well as distance and masses. The spins of individual black holes within a binary system introduce complexities in the emitted gravitational wave, influencing the amplitude, waveform modulation, and precession of the orbital plane. These spin-induced effects not only contribute to the quality of the observed signals but also impact the accuracy of parameter estimation, effective detection ranges of gravitational wave detectors, and the overall event rates [76, 72, 77]. BBH spins, particularly the effective spin χ_{eff} , are essential for extracting precise astrophysical information, providing valuable insights into the population properties and formation channels of binary black hole systems [78, 79]. The effective inspiral spin parameter χ_{eff} is defined as [27]

$$\chi_{\text{eff}} = \frac{(\vec{s}_1 m_1 + \vec{s}_2 m_2) \cdot \hat{\mathbf{L}}}{m_1 + m_2} \equiv \frac{m_1 s_{1z} + m_2 s_{2z}}{m_1 + m_2}, \quad (16)$$

where $\vec{s}_{1,2}$ are the (dimensionless) spins of each black hole and $\hat{\mathbf{L}}$ is the direction of the orbital angular momentum; this defines the spin projections along the orbital axis s_{1z}, s_{2z} .

Signals from binaries with $\chi_{\text{eff}} > 0$ (i.e. aligned spins) have a higher probability of detection, since their waveforms have a larger number of cycles and a higher duration in the detector sensitive band [27]; thus χ_{eff} should have a significant impact on the selection function [28, 80]. As mentioned previously, we compared cdfs of found injections, as well as histogramming them over various parameters, in order to study the dependence of P_{det}

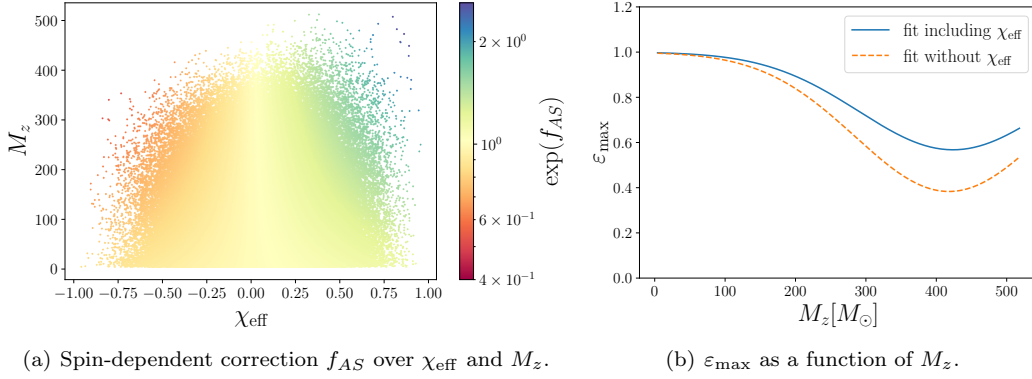


Figure 7. Search sensitivity dependencies for the fit including aligned spin effects. Panel (a) shows the correction to the sensitive distance, f_{AS} , over total redshifted mass and effective spin, for every O3 BBH injection. The comparison between the maximum search efficiency dependence on redshifted total mass from the fit with and without spin correction is shown in (b).

on χ_{eff} . Significant discrepancies were found with the previous fit function neglecting spins, Eqs. (9-11), verifying that the detection probability is an increasing function of χ_{eff} , an effect appearing stronger at higher total mass. Taking into account these discrepancies, spin dependence was implemented as follows:⁺

$$\tilde{d}_{\text{mid}} = D_0 \mathcal{M}_z^{5/6} \exp(f_d) \exp(f_{AS}), \quad (17)$$

$$f_{AS} = \chi_{\text{eff}}(c_{01} + c_{11}M_z). \quad (18)$$

We thus require to fit the coefficients c_{01} , c_{11} simultaneously with other parameters. Some changes to the likelihood are needed to account for the spin dependence $\chi_{\text{eff}}(m_1, m_2, s_{1z}, s_{2z})$: in place of Eqs. (12-14) we have:

$$\ln \mathcal{L} = -\mu + \sum_i \ln \lambda(d_L^i, m_1^i, m_2^i, s_{1z}^i, s_{2z}^i), \quad (19)$$

$$\lambda(d_L, m_1, m_2, s_{1z}, s_{2z}) = P_{\text{det}}(d_L, m_1, m_2, \chi_{\text{eff}}) p(d_L) p(m_1, m_2) p(s_{1z}, s_{2z}) N_{\text{tot}}, \quad (20)$$

$$\mu \equiv N_{\text{exp}} = \int \lambda(d_L, m_1, m_2, s_{1z}, s_{2z}) dm_1 dm_2 ds_{1z} ds_{2z} dd_L. \quad (21)$$

We find that the spin-dependent factor $\exp(f_{AS})$, shown in Fig. 7(a), is close to 1 for small values of χ_{eff} and small masses, but in the high mass limit, extreme values of the effective spin the correction can reduce d_{mid} by a factor of ~ 2 for the most negative values of χ_{eff} and increase it by a factor of ~ 2.5 for $\chi_{\text{eff}} \sim 1$. The spin correction also affected the fit of the maximum detection probability, as evident from Fig. 7(b). It is plausible that the lower values of ε_{max} from the fit neglecting spins were driven by the need to fit a mixture

⁺ Here the c subscripts represent powers of M_z and χ_{eff} .

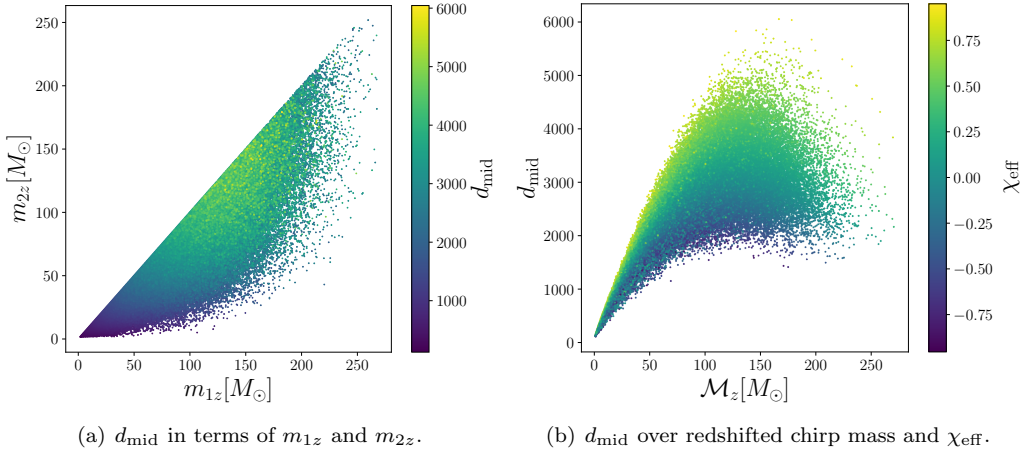


Figure 8. Sensitive distance d_{mid} values for the O3 BBH injections from the fit with spin dependence, over redshifted masses (a) and over redshifted chirp mass and effective spin (b).

of different d_{mid} values due to different spins at the same component mass point. The remaining apparent trend in ε_{max} is still subject to high uncertainties, explored in Sec. 5.

Figure 8(a) shows the d_{mid} values in terms of the redshifted masses from the new fit, where we can see that the maximum sensitive range increases by almost a factor of 2. In Fig. 8(b) we can see the effect of χ_{eff} in d_{mid} as a function of chirp mass: basically systems are detectable at higher distances the more aligned the spins are (the closer χ_{eff} is to 1) as expected. By comparison with Fig. 4(b), at fixed \mathcal{M}_z variations in χ_{eff} appear to have a larger effect on detectability than variations in η .

Lastly, we perform K-S tests to validate this new model with spin dependence. Figure 9 shows the cumulative found injections in the GWTC-3 catalog over χ_{eff} , along with the cdfs predicted by the selection function, for our fits both without the spin factor (a), and including it (b). A significant mismatch is visible in the fit without spin dependence. In general, the K-S statistic values over different variables obtained with the spin correction were 0.004 or less again, and p -values of 0.10 or larger, implying that the spin dependence is well fitted.

5. Statistical uncertainties in P_{det}

In order to quantify the statistical uncertainties in our estimation of the selection function, due to the finite number both of injections performed and, particularly, of found injections, we use a bootstrap resampling method. We randomly resample the observed data n times, allowing for replacements, and fit P_{det} to each bootstrap set of injections, thus obtaining n sets of optimized fit parameters. In addition to estimating the uncertainty on each fit parameter, bootstrap resampling fit allows us to assess how far uncertainties in the parameters are correlated with each other. Figure 10 illustrates the resulting uncertainty estimates in d_{mid} and ε_{max} over the detected total mass and the effective spin, by plotting

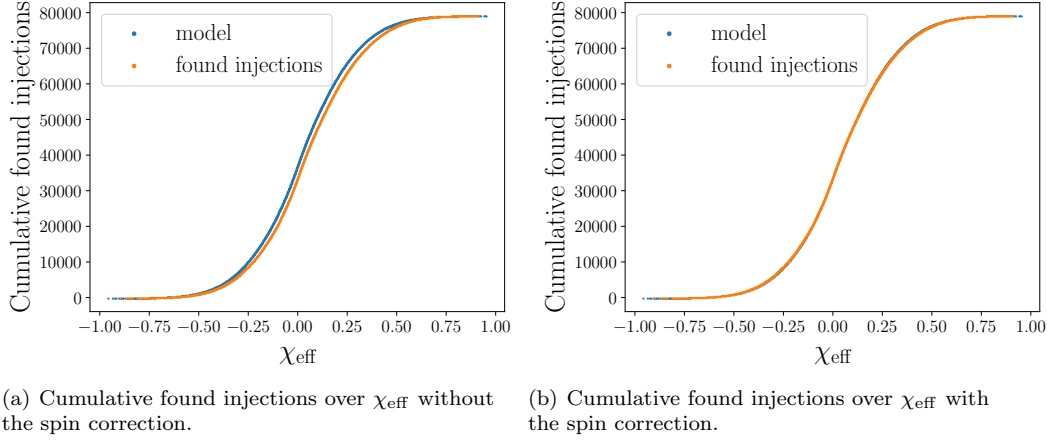


Figure 9. Comparative of the cumulative found injections over χ_{eff} from the GWTC-3 data (orange) and the predicted cdf from (15) (blue), without (a) and with (b) spin correction. The K-S statistics and p -values for the model without spin correction (a) are (0.0438, 0), and (0.0039, 0.19) for the new model (b).

$n = 100$ bootstrap iterations.

The results show that the estimated statistical uncertainty is lowest for low masses, becoming significant in the high mass limit; for a few bootstrap iterations we even see instability in the behaviour at very high total mass (over $\sim 200 M_{\odot}$) for unequal mass binaries, which we attribute to a very small number of found injections in this region. Figure 10(a) additionally shows that at fixed total mass the uncertainty decreases with increasing η , due to an increasing density of found injections. Figure 10(b), showing the uncertainty in d_{mid} as a function of effective spin for different values of the redshifted total mass, again demonstrates that uncertainties grow with M_z , but remain near-constant over χ_{eff} . Figure 10(c) shows the uncertainty in the dependence of ε_{max} on M_z : while there is a significant decrease from masses $100 M_{\odot}$ up to $350 - 400 M_{\odot}$, the behaviour at very high M_z is subject to large uncertainties, with a slight (not highly significant) trend to increasing ε_{max} .

Most of these trends are expected, as the number of detected injections in the high (redshifted) mass limit is very low. Obtaining useful sensitivity estimates in this regime will require a much higher density of injections here, allowing us to diagnose more clearly what factors may be causing the apparent increase in ε_{max} . It will be important to account for such uncertainties in any population analysis over this mass range; note that the main LVK O4 population analyses did not explore such high masses [14] given the lack of clear detections.

6. Discussion

In this work we have introduced a simple but accurate, physically motivated approximation of the detection probability P_{det} for binary merger signals in LIGO-Virgo-KAGRA search pipelines analyzing real gravitational-wave data, accounting for dependence on binary masses, orbit-aligned spins and luminosity distance. Observation selection bias, which is

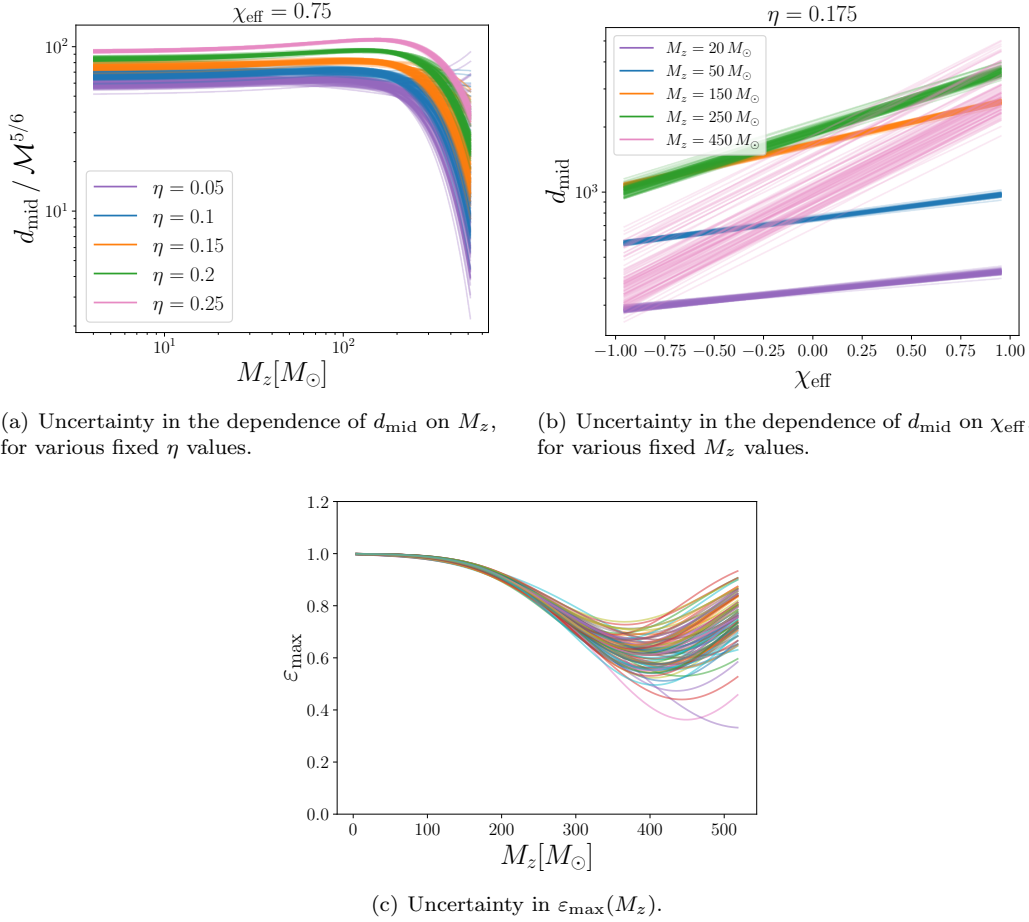


Figure 10. Uncertainty in P_{det} functions quantified via 100 bootstrap resampled analyses: each plotted line represents a bootstrap iteration.

quantified via this probability, has a very strong influence on the set of events recovered in any GW catalog, and thus must be taken into account in any kind of population analysis. The expected search sensitivity to a signal with given masses and spins depends on many diverse factors, including the distance and other extrinsic parameters, but also the detector sensitivities, data quality, and the configuration of search pipelines. These effects are most often accounted for by resampling (importance sampling) of simulated signals, i.e. injection sets, but this method is inefficient for general forms of population model, and may incur high uncertainties. Our proposed fit gives the probability of detection as a continuous (and differentiable) function over mass, spin and distance (or redshift), and thus makes it possible to do population studies using models of arbitrarily complex form without increased uncertainty in the selection function [47]. The fit may also be used for “forward modelling” to directly predict the number and distribution of observed events given the outputs of astrophysical population synthesis calculations.

Our fit function is motivated by the known dependence of the signal-to-noise ratio,

for a binary at fixed distance, on other parameters, mainly the sky location and binary orientation and the chirp mass. We allow for mass- and spin-dependent corrections to the theoretically expected behaviour: these corrections, as well as an overall scaling (related to the detector network sensitivity), are determined via a maximum-likelihood fit to the O3 injection campaign results. A surprisingly small number of correction terms is needed to obtain physically reasonable results which accurately predict of the number and distribution found injections, as verified by CDF comparisons and KS tests. The statistical uncertainty in the fitted P_{det} is small, except for the high (redshifted) mass and unequal mass limits where detected injections are very sparse. A limitation of our procedure (common to any empirical estimate of P_{det} from search results) is that we are unable to constrain or verify the behaviour of P_{det} outside the physical range of masses, distances and spins covered by the injection set, thus care is required if applying the fit in extreme cases such as the high mass limit. The limitation would of course be lifted by use of a wider injection parameter range.

A version of this fit (without including spin effects) was an essential ingredient for a nonparametric analysis of the evolution of the BBH population over redshift [21]. While we have concentrated on fitting the results of injections analyzed by search pipelines in real O3 data, the fitting method may also be applied to “semianalytic” injections associated with the O1 and O2 runs [81]. There are, however, significant differences relative to O3 in the method used for identifying these injections as detected – mainly, thresholding on optimal (expected) network SNR rather than on the search pipeline significance, i.e. false alarm rate (FAR) or ranking statistic, as well as the use of constant detector PSDs for each run. Although the resulting integrated sensitivity over O1 and O2 is consistent with total merger rate estimates, these method differences may produce a bias in the distance dependence of the “semianalytic” found injections, compared to what would be found by actual searches of O1 and O2 data with injections. Therefore, rather than a detailed functional fit of O1-O2 semianalytic injections, we instead recommend keeping the O3 fitted parameters, but scaling the d_{mid} values by a constant factor for each of the O1 and O2 runs (i.e. changing only D_0 between runs), such that the total counts of found injections for O1 and O2, and the numbers of actual BBH detections (3 and 10, respectively) are consistently predicted.

Although our method can already be used for investigations of the existing BBH population, characterized by near-equal masses, relatively low spin magnitudes and generally small or negligible precession effects, there are several possible extensions to its scientific scope. The next steps will be to include dependence over precessing BH spin components (i.e. those in the orbital plane), which are expected to influence search sensitivity, and also investigate the applicability of our fitting method in the mass ranges covered by BNS and NSBH injections.

Concerning methodological extensions, ways of marginalizing over or otherwise including uncertainties in P_{det} are to be investigated: for instance, when performing Bayesian analysis the fit parameters could be sampled over using the associated likelihood.* We are currently treating extrinsic angular parameters as unknowns to be averaged over: the form of our sigmoid function over distance in Eq. (4) is primarily determined by how the signal amplitude depends on such nuisance parameters. We expect that the probability of detection for a binary at a given distance *and with known sky location and orientation* will be related in a simple way to our fitted parametric form via d_{mid} . Including the explicit angular

* We thank Colm Talbot for this suggestion.

dependence may facilitate studies of any deviations from isotropy in the merging binary distribution (e.g. [82, 83]). Analogously, one could consider quantifying the dependence of P_{det} on the state of the detector network (rather than simply averaging over time), cf. [64], which may be of interest for detector characterization.

Acknowledgments

We are happy to acknowledge helpful discussions with the LVK Rates and Populations group, in particular Colm Talbot and Amanda Farah, and Vaibhav Tiwari for carefully reading an earlier version of this paper. This work has been supported by the Spanish Agencia Estatal de Investigación through the grant PRE2022-102569, funded by MCIN/AEI/10.13039/501100011033 and the FSE+. This work has received financial support from María de Maeztu grant CEX2023-001318-M funded by MICIU/AEI/10.13039/501100011033, and from the Xunta de Galicia (CIGUS Network of Research Centres) and the European Union. ALM and TD are supported by research grant PID2020-118635GB-I00 from the Spanish Ministerio de Ciencia e Innovación. This material is based upon work supported by NSF’s LIGO Laboratory which is a major facility fully funded by the National Science Foundation.

Data availability

The data that support the findings of this study are openly available at the following URLs: https://github.com/AnaLorenzoMedina/cbc_pdet, <https://zenodo.org/records/7890437>.

References

- [1] Abbott B P *et al.* (LIGO Scientific, Virgo) 2016 *Phys. Rev. Lett.* **116** 061102
- [2] Cutler C and Flanagan E E 1994 *Phys. Rev. D* **49** 2658–2697
- [3] Abbott R *et al.* (KAGRA, VIRGO, LIGO Scientific) 2023 *Phys. Rev. X* **13** 041039 (*Preprint* 2111.03606)
- [4] Fishbach M and Kalogera V 2022 *Astrophys. J. Lett.* **929** L26 (*Preprint* 2111.02935)
- [5] Belczynski K, Done C, Hagen S, Lasota J P and Sen K 2024 *Astron. Astrophys.* **690** A21 (*Preprint* 2111.09401)
- [6] Spera M, Trani A A and Mencagli M 2022 *Galaxies* **10** 76 (*Preprint* 2206.15392)
- [7] Belczynski K *et al.* 2020 *Astron. Astrophys.* **636** A104
- [8] Stevenson S, Vigna-Gómez A, Mandel I, Barrett J W, Neijssel C J, Perkins D and de Mink S E 2017 *Nature Commun.* **8** 14906
- [9] Rodriguez C L, Chatterjee S and Rasio F A 2016 *Phys. Rev. D* **93** 084029
- [10] O’Leary R M, Meiron Y and Kocsis B 2016 *Astrophys. J. Lett.* **824** L12
- [11] McKernan B *et al.* 2018 *Astrophys. J.* **866** 66
- [12] Belczynski K, Romagnolo A, Olejak A, Klencki J, Chattopadhyay D, Stevenson S, Miller M C, Lasota J P and Crowther P A 2022 *Astrophys. J.* **925** 69 (*Preprint* 2108.10885)
- [13] Abbott R *et al.* (LIGO Scientific, Virgo) 2021 *Astrophys. J. Lett.* **913** L7 (*Preprint* 2010.14533)
- [14] Abbott R *et al.* (KAGRA, VIRGO, LIGO Scientific) 2023 *Phys. Rev. X* **13** 011048 (*Preprint* 2111.03634)
- [15] Abbott B P *et al.* (LIGO Scientific, Virgo) 2016 *Astrophys. J. Lett.* **818** L22
- [16] Zevin M, Bavera S S, Berry C P L, Kalogera V, Fragos T, Marchant P, Rodriguez C L, Antonini F, Holz D E and Pankow C 2021 *Astrophys. J.* **910** 152 (*Preprint* 2011.10057)
- [17] Fishbach M, Doctor Z, Callister T, Edelman B, Ye J, Essick R, Farr W M, Farr B and Holz D E 2021 *Astrophys. J.* **912** 98 (*Preprint* 2101.07699)
- [18] Tiwari V 2022 *Astrophys. J.* **928** 155 (*Preprint* 2111.13991)

- [19] Karathanasis C, Mukherjee S and Mastrogianni S 2023 *Mon. Not. Roy. Astron. Soc.* **523** 4539–4555 (*Preprint* 2204.13495)
- [20] Biscoveanu S, Callister T A, Haster C J, Ng K K Y, Vitale S and Farr W M 2022 *Astrophys. J. Lett.* **932** L19 (*Preprint* 2204.01578)
- [21] Rinaldi S, Del Pozzo W, Mapelli M, Lorenzo-Medina A and Dent T 2024 *Astron. Astrophys.* **684** A204 (*Preprint* 2310.03074)
- [22] Mapelli M, Bouffanais Y, Santoliquido F, Sedda M A and Artale M C 2022 *Mon. Not. Roy. Astron. Soc.* **511** 5797–5816 (*Preprint* 2109.06222)
- [23] van Son L A C, de Mink S E, Callister T, Justham S, Renzo M, Wagg T, Broekgaarden F S, Kummer F, Pakmor R and Mandel I 2022 *Astrophys. J.* **931** 17 (*Preprint* 2110.01634)
- [24] Belczynski K, Doctor Z, Zevin M, Olejak A, Banerje S and Chattopadhyay D 2022 *Astrophys. J.* **935** 126 (*Preprint* 2204.11730)
- [25] Ng K K Y, Vitale S, Farr W M and Rodriguez C L 2021 *Astrophys. J. Lett.* **913** L5 (*Preprint* 2012.09876)
- [26] Abadie J, Abbott B P *et al.* 2010 *Classical and Quantum Gravity* **27** 173001
- [27] Ajith P, Hannam M, Husa S, Chen Y, Brüggmann B, Dorband N, Müller D, Ohme F, Pollney D, Reisswig C, Santamaría L and Seiler J 2011 *Phys. Rev. Lett.* **106**(24) 241101
- [28] Ng K K, Vitale S, Zimmerman A, Chatziioannou K, Gerosa D and Haster C J 2018 *Physical Review D* **98**
- [29] Harry I, Privitera S, Bohé A and Buonanno A 2016 *Phys. Rev. D* **94** 024012 (*Preprint* 1603.02444)
- [30] Capano C, Pan Y and Buonanno A 2014 *Phys. Rev. D* **89** 102003 (*Preprint* 1311.1286)
- [31] Harry I, Calderón Bustillo J and Nitz A 2018 *Phys. Rev. D* **97** 023004 (*Preprint* 1709.09181)
- [32] Brown D A and Zimmerman P J 2010 *Phys. Rev. D* **81** 024007 (*Preprint* 0909.0066)
- [33] Gadre B, Soni K, Tiwari S, Ramos-Buades A, Haney M and Mitra S 2024 (*Preprint* 2405.04186)
- [34] Romero-Shaw I M, Gerosa D and Loutrel N 2023 *Mon. Not. Roy. Astron. Soc.* **519** 5352–5357 (*Preprint* 2211.07528)
- [35] Allen B, Anderson W G, Brady P R, Brown D A and Creighton J D E 2012 *Phys. Rev. D* **85** 122006 (*Preprint* gr-qc/0509116)
- [36] Usman S A *et al.* 2016 *Class. Quant. Grav.* **33** 215004 (*Preprint* 1508.02357)
- [37] Messick C *et al.* 2017 *Phys. Rev. D* **95** 042001 (*Preprint* 1604.04324)
- [38] Adams T, Buskulic D, Germain V, Guidi G M, Marion F, Montani M, Mours B, Piergiorganni F and Wang G 2016 *Class. Quant. Grav.* **33** 175012 (*Preprint* 1512.02864)
- [39] Luan J, Hooper S, Wen L and Chen Y 2012 *Phys. Rev. D* **85** 102002 (*Preprint* 1108.3174)
- [40] Banagiri S, Berry C P L, Cabourn Davies G S, Tsukada L and Doctor Z 2023 *Phys. Rev. D* **108** 083043 (*Preprint* 2305.00071)
- [41] Lukina O and Davis D 2023 Understanding combined results from multiple GW searches using information theory Tech. rep. LIGO SURF <https://dcc.ligo.org/LIGO-T2300203/public>
- [42] Mandel I, Farr W M and Gair J R 2019 *Mon. Not. Roy. Astron. Soc.* **486** 1086–1093 (*Preprint* 1809.02063)
- [43] Farr W M 2019 *Research Notes of the AAS* **3** 66 URL <https://dx.doi.org/10.3847/2515-5172/ab1d5f>
- [44] Press W H, Teukolsky S A, Vetterling W T and Flannery B P 1986 *Numerical Recipes: The Art of Scientific Computing* (Cambridge University Press) <https://numerical.recipes/>
- [45] Tiwari V 2018 *Class. Quant. Grav.* **35** 145009 (*Preprint* 1712.00482)
- [46] Essick R and Farr W 2022 (*Preprint* 2204.00461)
- [47] Talbot C and Golomb J 2023 *Mon. Not. Roy. Astron. Soc.* **526** 3495–3503 (*Preprint* 2304.06138)
- [48] Galaudage S *et al.* 2021 *Astrophys. J. Lett.* **921** L15 [Erratum: *Astrophys.J.Lett.* 936, L18 (2022)] (*Preprint* 2109.02424)
- [49] Chatterjee S and Diaconis P 2018 *The Annals of Applied Probability* **28** 1099–1135 (*Preprint* 1511.01437)
- [50] Fishbach M and Holz D E 2017 *Astrophys. J. Lett.* **851** L25 (*Preprint* 1709.08584)
- [51] Essick R 2023 *Phys. Rev. D* **108** 043011 (*Preprint* 2307.02765)
- [52] Gerosa D and Bellotti M 2024 *Class. Quant. Grav.* **41** 125002 (*Preprint* 2404.16930)
- [53] Davies G S, Dent T, Tápai M, Harry I, McIsaac C and Nitz A H 2020 *Phys. Rev. D* **102** 022004 (*Preprint* 2002.08291)
- [54] Sachdev S *et al.* 2019 (*Preprint* 1901.08580)
- [55] Aubin F *et al.* 2021 *Classical and Quantum Gravity* **38** 095004
- [56] Davies G S C and Harry I W 2022 *Class. Quant. Grav.* **39** 215012 (*Preprint* 2203.08545)
- [57] Davis D *et al.* (LIGO) 2021 *Class. Quant. Grav.* **38** 135014 (*Preprint* 2101.11673)
- [58] Acernese F *et al.* (Virgo) 2023 *Class. Quant. Grav.* **40** 185006 (*Preprint* 2210.15633)
- [59] Zackay B, Venumadhav T, Roulet J, Dai L and Zaldarriaga M 2021 *Phys. Rev. D* **104** 063034 (*Preprint*

- 1908.05644)
- [60] Mozzon S, Nuttall L K, Lundgren A, Dent T, Kumar S and Nitz A H 2020 *Class. Quant. Grav.* **37** 215014 (*Preprint* 2002.09407)
 - [61] Tsukada L *et al.* 2023 *Physical Review D* **108**
 - [62] Kumar P and Dent T 2024 *Phys. Rev. D* **110** 043036 (*Preprint* 2403.10439)
 - [63] Dent T and Veitch J 2014 *Phys. Rev. D* **89** 062002 (*Preprint* 1311.7174)
 - [64] Essick R, Godwin P, Hanna C, Blackburn L and Katsavounidis E 2020 (*Preprint* 2005.12761)
 - [65] Godwin P *et al.* 2020 (*Preprint* 2010.15282)
 - [66] Davis D, Trevor M, Mozzon S and Nuttall L K 2022 *Phys. Rev. D* **106** 102006 (*Preprint* 2204.03091)
 - [67] Wysocki D, Lange J and O'Shaughnessy R 2019 *Phys. Rev. D* **100** 043012 (*Preprint* 1805.06442)
 - [68] Talbot C and Thrane E 2022 *Astrophys. J.* **927** 76 (*Preprint* 2012.01317)
 - [69] LIGO Scientific, Virgo and KAGRA Collaborations 2021 GWTC-3: Compact Binary Coalescences Observed by LIGO and Virgo During the Second Part of the Third Observing Run – O3 search sensitivity estimates URL <https://doi.org/10.5281/zenodo.5546676>
 - [70] LIGO Scientific, Virgo and KAGRA Collaborations 2021 Gwtc-3 data release <https://www.gw-openscience.org/GWTC-3>
 - [71] Finn L S and Chernoff D F 1993 *Physical Review D* **47** 2198–2219
 - [72] Dal Canton T, Lundgren A P and Nielsen A B 2015 *Physical Review D* **91**
 - [73] Bezdek J C and Hathaway R J 2002 Some notes on alternating optimization *Advances in Soft Computing — AFSS 2002* ed Pal N R and Sugeno M (Berlin, Heidelberg: Springer Berlin Heidelberg) pp 288–300
 - [74] Lagarias J C, Reeds J A, Wright M H and Wright P E 1998 *SIAM Journal on Optimization* **9** 112–147
 - [75] Martynov D V *et al.* 2016 *Phys. Rev. D* **93**(11) 112004
 - [76] van der Sluys M V, Röver C, Stroeer A, Raymond V, Mandel I, Christensen N, Kalogera V, Meyer R and Vecchio A 2008 *The Astrophysical Journal* **688** L61–L64
 - [77] Hotokezaka K and Piran T 2017 *The Astrophysical Journal* **842** 111
 - [78] Tong H, Galadage S and Thrane E 2022 *Phys. Rev. D* **106** 103019 (*Preprint* 2209.02206)
 - [79] Nishizawa A, Berti E, Klein A and Sesana A 2016 *Physical Review D* **94**
 - [80] Hoy C, Fairhurst S, Hannam M and Tiwari V 2022 *Astrophys. J.* **928** 75 (*Preprint* 2110.13542)
 - [81] LIGO Scientific, Virgo and KAGRA Collaborations 2023 GWTC-3: Compact Binary Coalescences Observed by LIGO and Virgo During the Second Part of the Third Observing Run – O1+O2+O3 Search Sensitivity Estimates URL <https://doi.org/10.5281/zenodo.7890398>
 - [82] Stiskalek R, Veitch J and Messenger C 2021 *Mon. Not. Roy. Astron. Soc.* **501** 970–977 (*Preprint* 2003.02919)
 - [83] Payne E, Banagiri S, Lasky P and Thrane E 2020 *Phys. Rev. D* **102** 102004 (*Preprint* 2006.11957)
 - [84] Fishbach M, Holz D E and Farr W M 2018 *The Astrophysical Journal* **863** L41
 - [85] Hogg D W 1999 (*Preprint* astro-ph/9905116)
 - [86] Baes M, Camps P and Putte D V D 2017 *Monthly Notices of the Royal Astronomical Society* **468** 927–930
 - [87] Planck Collaboration *et al.* 2016 *Astronomy & Astrophysics* **594** A13

Appendix A. Injection probability density functions

In this Appendix we summarize the PDFs of the O3 injected BBH signal distribution over the relevant binary parameters [69]. The source-frame mass distribution is parameterized as power laws in the two component masses:

$$p(m_1, m_2) = p(m_1)p(m_2|m_1), \quad (\text{A.1})$$

with the restriction that $m_2 \leq m_1$ and

$$p(m_1) \sim m_1^\alpha, \quad m_{1,min} \leq m_1 \leq m_{1,max}, \quad (\text{A.2})$$

$$p(m_2|m_1) \sim m_2^\beta, \quad m_{2,min} \leq m_2 \leq m_1. \quad (\text{A.3})$$

The BBH injection distribution for the GWTC-3 catalog [3] uses $\alpha = -2.53$, $\beta = 1$, $m_{1,min} = m_{2,min} = 2 M_\odot$ and $m_{1,max} = m_{2,max} = 100 M_\odot$. By normalizing (A.1) to 1, we obtain the explicit mass distribution

$$p(m_1, m_2) = m_1^\alpha m_2^\beta \frac{\alpha + 1}{m_{max}^{\alpha+1} - m_{min}^{\alpha+1}} \frac{\beta + 1}{m_1^{\beta+1} - m_{min}^{\beta+1}}, \quad m_2 \leq m_1. \quad (\text{A.4})$$

This distribution is normalized over the whole space; however, in the context of our mass binned fitting (Sec. 2.2), we require PDFs normalized over each bin separately. Since the relevant integrals are straightforward we do not give the normalizations explicitly. Note that for bins crossing the equal-mass line ($m_1 = m_2$) precautions are needed, as since half of the bin area has $m_2 > m_1$ and thus does not contain injections.

The redshift distribution used follows the proposal in [84]:

$$p(z) = \frac{dV_c}{dz} (1+z)^{\kappa-1} \quad z \leq z_{max}, \quad (\text{A.5})$$

where V_c is the contained comoving volume corresponding to a redshift z defined by a flat Λ CDM cosmology. For BBH injections, $z_{max} = 1.9$ and $\kappa = 1$. The luminosity distance is related to the cosmological redshift z in flat Lambda-Cold Dark Matter (Λ CDM) cosmology [85, 86] via the comoving distance d_C as

$$d_L(z) = (1+z)d_C = (1+z) \frac{c}{H_0} \int_0^z \frac{dt}{\sqrt{\Omega_m(1+t)^3 + (1-\Omega_m)}}, \quad (\text{A.6})$$

where we take $H_0 = 67.9 \text{ km/s/Mpc}$, $\Omega_m = 0.3065$ and $\Omega_\Lambda = 1 - \Omega_m = 0.6935$ (following [87]). The luminosity distance PDF will be

$$p(d_L) = \frac{p(z)}{d(d_L)/dz} = p(z) \left[d_C + \frac{c}{H_0} \frac{(1+z)}{\sqrt{\Omega_m(1+z)^3 + (1-\Omega_m)}} \right]^{-1}. \quad (\text{A.7})$$

Finally, the spin distribution is defined over Cartesian spin components for each binary component: the magnitude of each spin is uniformly distributed between zero and the maximum value s_{\max} and the spin directions are isotropic, thus

$$p(s_x, s_y, s_z) = \frac{1}{4\pi(s_x^2 + s_y^2 + s_z^2)s_{\max}} \quad , \quad s_x^2 + s_y^2 + s_z^2 \leq s_{\max}^2. \quad (\text{A.8})$$